

Representing Mesoscale Variability in Superparameterized Climate models

Fredrik Jansson^{1,2}, Gijs van den Oord³, Inti Pelupessy³, Maria Chertova³, Johanna H.
Grönqvist⁴, A. Pier Siebesma^{1,5}, Daan Crommelin^{2,6}

¹Delft University of Technology, Delft, Netherlands

²Centrum Wiskunde & Informatica, Amsterdam, Netherlands

³Netherlands eScience Center, Amsterdam, Netherlands

⁴Department of Physics, Åbo Akademi University, Turku, Finland

⁵Royal Netherlands Meteorological Institute, de Bilt, Netherlands

⁶Korteweg-de Vries Institute for Mathematics, University of Amsterdam, Amsterdam, Netherlands

Key Points:

- Superparameterization in weather models is used to improve the representation of clouds
- We show that superparameterization suppresses the transport of clouds
- A scheme for controlling the humidity variation improves cloud advection in superparameterized models

Corresponding author: Fredrik Jansson, fjansson@abo.fi

Abstract

In atmospheric modeling, superparameterization has gained popularity as a technique to improve cloud and convection representations in large scale models, by coupling them locally to cloud-resolving models. We show how the different representations of cloud water in the local and the global models in superparameterization lead to a suppression of cloud advection and ultimately to a systematic underrepresentation of the cloud amount in the large scale model. We demonstrate this phenomenon in a regional superparameterization experiment with the global model OpenIFS coupled to the local model DALES (the Dutch Atmospheric Large Eddy Simulation), as well as in an idealized setup, where the large-scale model is replaced by a simple advection scheme. To mitigate the problem of suppressed cloud advection, we propose a scheme where the spatial variability of the local model's total water content is enhanced in order to achieve the correct cloud condensate amount.

Plain Language Summary

In this article we investigate a technique called superparameterization for improving how global weather and climate models represent clouds and convection. In current operational global weather and climate models, the resolution is limited to 10–100 km by computational resources. This is not sufficient to resolve cloud and convective processes. The effect of these processes must then be approximated by so-called parameterizations. Superparameterization uses another, local atmospheric model with a higher resolution, nested inside the columns of the global model, to evaluate the effects of clouds and convection. By analysing results from a superparameterized simulation, we show that superparameterization as it is generally implemented suppresses advection of existing clouds from one grid column to another in the global model, leading to a severe underestimation of the amount of shallow clouds. The suppression occurs because the global and local models represent clouds in different ways, and the commonly used superparameterization scheme does not communicate the full cloud information from the global model to the local one. Adding such a coupling of the cloud information to the superparameterization scheme improves the advection of clouds.

1 Introduction

Many of the systematic biases and uncertainties in conventional general circulation models (GCMs) can be attributed to the highly parameterized representation of clouds, turbulence and convection. It is even questionable whether these biases will be eliminated unless resolutions of GCMs become fine enough for these processes to be numerically resolved. As pointed out by *Arakawa et al.* [2011, 2016] there are essentially two possible routes toward such global large eddy models (GLEMs).

Route 1 follows the traditional approach of continuously refining the resolution until clouds, convection and turbulence are sufficiently resolved. This requires scale aware parameterizations for these processes that are gradually switched off with increasing resolution in a physically consistent manner. Alternatively one can make large jumps in the used resolution so certain parameterizations can be switched off abruptly. At present, a horizontal resolution of around 1 km is the highest possible resolution for subseasonal global simulations of the atmosphere [*Stevens et al.*, 2019a; *Sato et al.*, 2019]. For such storm resolving resolutions, the general belief is that deep moist convective overturning is sufficiently well resolved to the extent that any additional deep convection parameterization will deteriorate the skill of the simulation. Obviously, at these storm resolving resolutions there is still a turbulence parameterization required as well as some parameterized representation of boundary layer cloudiness and shallow cumulus convection.

65 Route 2 makes use of a “multi-scale modeling framework” (MMF). In its original
66 form, deep moist convection parameterization was replaced (or “superparameterized”)
67 by a 2D storm resolving model (2D SRM) in each cell of a GCM [*Grabowski and Smo-*
68 *larkiewicz, 1999; Grabowski, 2001*]. More recently, the use of a 3D large eddy model
69 as a superparameterization (SP) for clouds, convection and turbulence has been proposed
70 [*Grabowski, 2016; Parishani et al., 2017; Jansson et al., 2019*]. This approach has the ad-
71 vantage that most of the small scale dynamics and cloud microphysics is well represented
72 while the GCM can still be formulated in an efficient hydrostatic manner. Further com-
73 putational advantages of this approach over a GLEM are discussed in *Grabowski [2016]*.
74 Because the use of a 3D large eddy model as a superparameterization on a global scale is
75 computationally not yet feasible, *Jansson et al. [2019]* implemented the possibility of using
76 a 3D Large Eddy Model (LEM) on a regional scale in the global Integrated Forecasting
77 System (IFS) of the ECMWF [*Malardel et al., 2016*]. This implies that a number of grid
78 cells in the IFS can be selected to be superparameterized while the remaining part of the
79 IFS will use the conventional parameterizations for clouds, convection and turbulence. In
80 the study by *Jansson et al. [2019]* the implementation of the Dutch Atmospheric Large
81 Eddy Simulation (DALES, *Heus et al. [2010]*) model as a superparameterization into the
82 IFS was documented, along with a case study of local shallow cumulus convection over
83 land to demonstrate the potential of this approach.

84 Despite the many advantages, the MMF does not come without problems. One draw-
85 back of this approach is that the communication between neighboring GCM cells can only
86 occur by the advection of the variables of the GCM. Therefore it is not possible in the su-
87 perparameterized framework to advect a spatial structure, as resolved by a local LEM, to a
88 neighboring GCM grid cell — only the mean state of a GCM grid cell can be advected to
89 a neighboring cell. In other words, the MMF introduces a scale break as it does not allow
90 structures, or even variability, to grow upscale to scales beyond the size of the GCM grid
91 size. Another related but more severe drawback of the MMF follows from the fact that
92 while most GCMs carry separate prognostic variables for the water vapor and the water
93 in the condensed phase, this is not the case for the local LEM. Most local models use the
94 total water specific humidity q_t , i.e the sum of water vapor and the condensed water, as
95 a prognostic variable. This implies that while the GCM separately advects the amount of
96 condensed water and water vapor from one grid cell to a neighboring one, the local LEM
97 of the neighboring cell is incapable of digesting this information and can only take the
98 sum of the advected vapor and condensed water as input.

99 As will be demonstrated in detail, this implies that a cloud which is advected to a
100 neighboring grid cell by the GCM will be directly diluted and dissipated in the local LEM
101 of the neighbouring cell. This dissipation of advected clouds is likely a general problem
102 in all published studies of superparameterizations that make use of SRMs with total water
103 specific humidity as a prognostic variable.

104 In short, the main purpose of this paper is i) to show that most superparameteriza-
105 tions as they are used today dissipate most of the advected cloud condensate, leading to
106 strong underestimation of cloud condensate and ii) to offer a simple solution by advecting
107 the appropriate variance of humidity between GCM grid cells that are commensurate with
108 the advected cloud condensate.

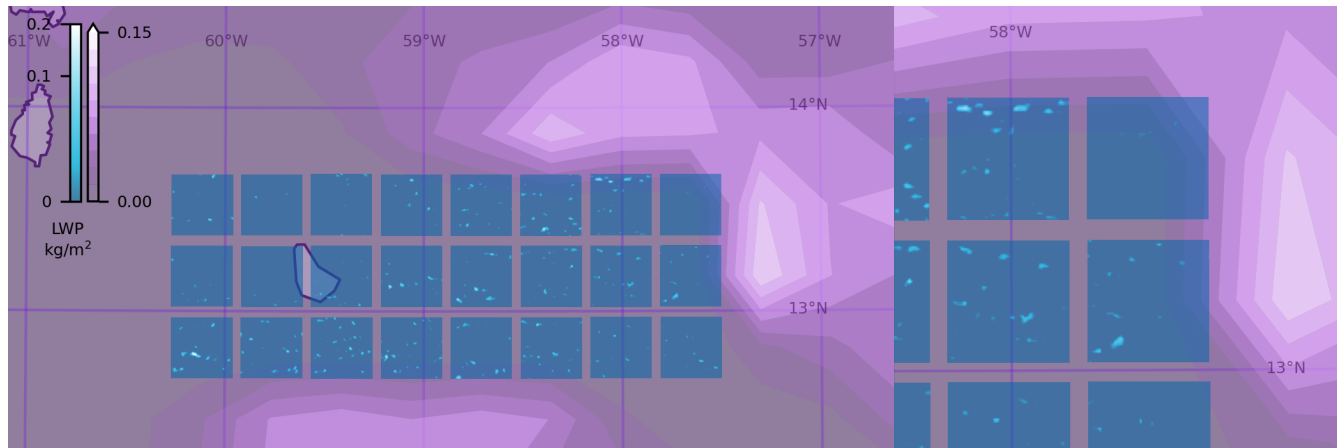
109 The paper is organised as follows. In section 2, we analyse the SP procedure and
110 its consequences for cloud advection. As an example, we show a regional SP simulation
111 with the LEMs located over the subtropical Northern Atlantic Ocean, in the vicinity of
112 Barbados. The example shows almost complete suppression of cloud advection into the
113 superparameterized region. In section 3 we propose an extension of the SP scheme with a
114 procedure to adjust the small-scale variability in the local models, in order to better pre-
115 serve the cloud condensate. In section 4 we present an idealized SP experiment where the
116 large-scale model consists of only advection, to demonstrate the lack of cloud advection in
117 SP and to see the impact of the variability coupling scheme in a simple setup. The effects

118 of the variability coupling procedure on the full Barbados simulation is evaluated in sec-
 119 tion 5. In the concluding section 6 we discuss the impact of the cloud advection issue on
 120 SP experiments.

121 2 Suppressed cloud advection in superparameterization

122 In this section, we show that a SP scheme can lead to suppressed advection of cloud
 123 condensate in the large-scale model.

124 2.1 Superparameterized Barbados experiment



125 **Figure 1.** A superparameterized simulation over Barbados on 2013-12-15 at 9:30 UTC, showing that in-
 126 coming clouds in the large-scale (purple) model do not easily advect into the superparameterized region (blue
 127 boxes). The right hand-image shows a magnification of the eastern (upwind) part of the SP region.

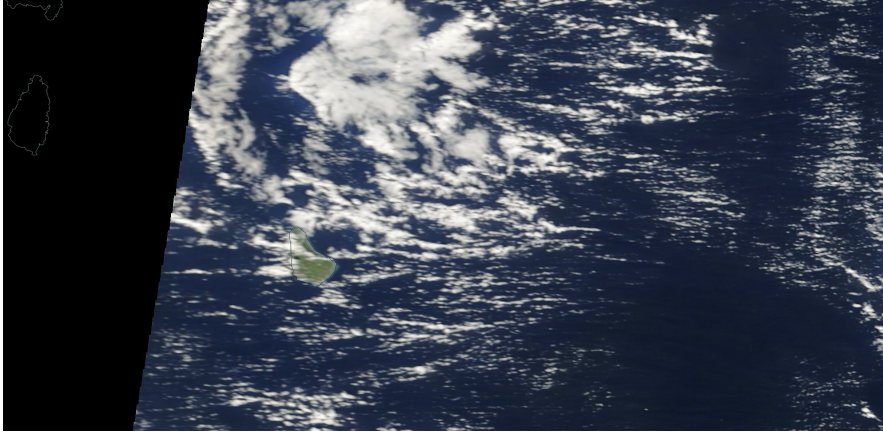
128 We demonstrate this lack of cloud advection in an experiment with the regional SP
 129 of OpenIFS with DALES [Jansson *et al.*, 2019], with the SP region located over Barbados,
 130 as shown in figure 1. This case has a wind from the east which brings clouds into the
 131 superparameterized region. A satellite image of the same area is shown in figure 2.

132 The region features persistent shallow cumulus clouds transported by the trade winds,
 133 with cloud patterns and cloud organizations occurring on widely different length scales.
 134 It is an interesting test case for SP, in particular to investigate how well SP represents
 135 cloud organization. The time and the location were chosen to coincide with the NARVAL
 136 [Stevens *et al.*, 2019b] observation campaign. The location is also part of the recent EU-
 137 REC4A campaign [Bony *et al.*, 2017; Stevens *et al.*, 2021].

139 Figure 3 shows the liquid water path and total water path in the GCM from the SP
 140 simulation mentioned above, compared to a corresponding simulation without SP, i.e. us-
 141 ing the standard OpenIFS. The SP columns show virtually no clouds as opposed to the
 142 neighboring columns. The figure shows that the total water path in the two simulations are
 143 similar, while the liquid water path is markedly lower in the SP columns.

151 We will argue that the reason for the lack of clouds in the SP columns is because
 152 advection of clouds into the SP columns is suppressed by the SP coupling.

153 This cloud suppression issue is especially visible in a regional SP model where the
 154 global model contains both superparameterized and regular columns next to each other as



138 **Figure 2.** Satellite image from Terra/MODIS over the same region as figure 1, on 2013-12-15 13:55 UTC.

155 illustrated in Fig. 3. The problem is not, however, restricted to regional superparameteri-
 156 zations but can be expected also in uniformly superparameterized models.

157 **2.2 Model coupling in superparameterization**

158 For the physical model coupling between a LEM or another local model and some
 159 or all columns of a GCM, we have followed the same approach as described by *Grabowski*
 160 [2004]. Since this coupling plays a crucial role in the cloud suppression, we briefly review
 161 the procedure here.

162 The general idea is that for each coupled variable, a forcing is introduced, which
 163 keeps the states of the two models consistent with each other,

$$\Phi(X, Y, Z, t) = \langle \phi(x, y, z, t) \rangle. \quad (1)$$

164 The brackets $\langle \cdot \rangle$ here denote a spatial average over the LEM domain in the horizontal di-
 165 rections. Capital letters denote variables in the GCM, small letters denote variables used
 166 in the LEM. Φ and ϕ here may represent any of the prognostic variables. The details of
 167 the regional SP setup used here are given in *Jansson et al.* [2019]; we here give the cou-
 168 pling equations for reference.

169 The GCM first performs a single time step from time T to $T + \Delta T$, after which the
 170 LEM is evolved over the same time interval, in multiple smaller time steps of length Δt .
 171 Before the time evolution of each model, forcings are calculated based on the difference
 172 between the most recently obtained states of the two models, chosen such as to keep equa-
 173 tion (1) satisfied. The coupling and the time stepping of the system are described in the
 174 following 4 steps.

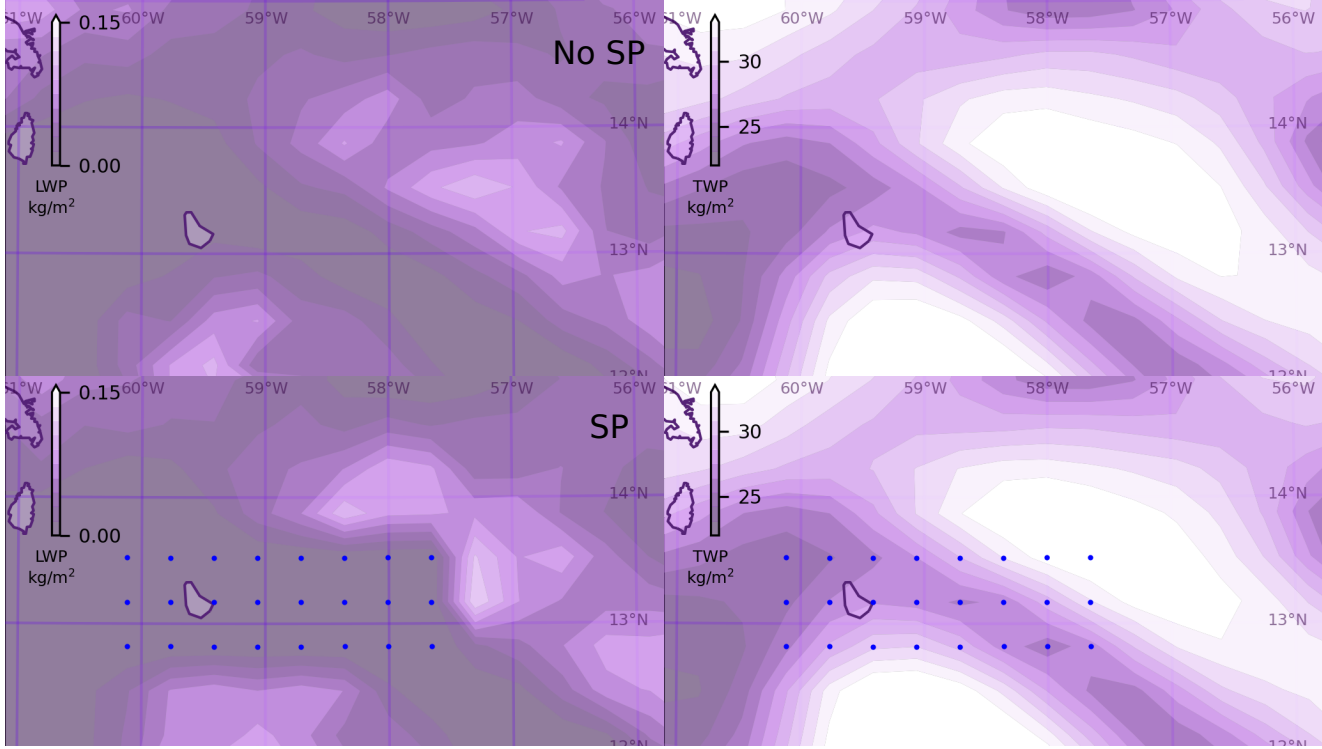
- 175 (i) Given the state of both models at time T , represented by $\Phi(T)$ for any of the GCM
 176 variables and $\phi(T)$ for the corresponding LEM variable, the forcing F_Φ on the vari-
 177 able Φ in the GCM is calculated as

$$F_\Phi(T) = \frac{\langle \phi(T) \rangle - \Phi(T)}{\Delta T}. \quad (2)$$

- 178 (ii) Time-step the GCM

$$\Phi(T + \Delta T) = \Phi(T) + \Delta T [A_\Phi(T) + S_\Phi(T) + F_\Phi(T)], \quad (3)$$

179 where $A_\Phi(T)$ represents advection terms and $S_\Phi(T)$ represents source terms for the
 180 variable Φ during the step from T to $T + \Delta T$.



144 **Figure 3.** Comparing dynamics of the liquid water path and total water path in standard OpenIFS (top)
 145 and an SP setup (bottom), in a simulation over Barbados. Superparameterized grid columns are marked with
 146 blue dots. The wind is from the east, advecting clouds in to the superparameterized regions. In the normal
 147 superparameterization, there is a hole in the cloud cover (seen in the liquid water path (LWP, left)
 148 over the superparameterized region, compared to standard OpenIFS. The total water path (TWP, right) is similar be-
 149 tween the two simulations, and does not show different behaviour in the superparameterized columns. The
 150 simulation was initialized on 2013-12-15 at 00 UTC, the image shows the state at 09:30.

181 (iii) Now the forcing on ϕ in the LEM is calculated as

$$f_{\phi}(T) = \frac{\Phi(T + \Delta T) - \langle \phi(T) \rangle}{\Delta T}. \quad (4)$$

182 (iv) and finally the time-step the LEM is executed as

$$\phi(T + \Delta T) = \phi(T) + \sum_{t=T}^{T+\Delta T} \Delta t [a_{\phi}(t) + s_{\phi}(t) + f_{\phi}(T)]. \quad (5)$$

183 The sums over t here represent evolving the LEM over several time steps, with
 184 $a_{\phi}(t)$ denoting advection terms and $s_{\phi}(t)$ denoting source terms for ϕ .

185 2.3 Coupling of DALES and OpenIFS

190 The SP of OpenIFS with DALES is formulated with couplings of variables for the
 191 horizontal wind velocities, temperature, and humidity. A summary of the coupling is pro-
 192 vided in table 1. While OpenIFS uses the regular temperature T as a variable, DALES is
 193 formulated using the liquid water potential temperature θ_l ,

$$\theta_l \approx \frac{T}{\Pi(p)} - \frac{L}{c_{pd}\Pi(p)} q_c. \quad (6)$$

Coupled variables

OpenIFS	direction	DALES	description
U, V	\leftrightarrow	u, v	horizontal velocity
T	\leftrightarrow	θ_l	temperature / liquid water potential temperature
$Q_V + Q_L + Q_I$	\rightarrow	q_t	specific total humidity
Q_V	\leftarrow	$q_t - q_c$	specific water vapor humidity
Q_L, Q_I	\leftarrow	q_c	specific condensed water humidity

Table 1. Summary of the coupling of OpenIFS and DALES. U and V are horizontal velocities, T is the temperature in OpenIFS, and θ_l is the liquid water potential temperature in DALES. Q_V , Q_L and Q_I are the specific water vapor, cloud liquid, and cloud ice amounts in OpenIFS, while q_t and q_c are the specific total water and cloud condensate amounts in DALES.

where q_c is the specific cloud condensed water content and $c_{pd} \approx 1004 \text{ J/kg K}$ is the specific heat of dry air at constant pressure. The Exner function $\Pi(p)$ is defined as

$$\Pi(p) = \left(\frac{p}{p_0} \right)^{R_d/c_{pd}}, \quad (7)$$

where $L \approx 2.5 \cdot 10^6 \text{ J/kg}$ is the latent heat of water vaporization, and $R_d \approx 287.04 \text{ J/kg K}$ is the gas constant for dry air.

In the experiments shown here, IFS was operating at an effective horizontal resolution of 40 km (T511L91 grid), while the DALES domains cover $12.8 \times 12.8 \text{ km}$ with a resolution of 200 m. Further details are given in [Jansson *et al.*, 2019].

2.4 Representation of clouds and small-scale variability

In this section we will show how the different representations of clouds in the GCM and the LEM lead to an insufficient coupling of cloud quantities in SP and reduced advection of existing clouds into SP columns.

While the SP coupling described above conserves the amount of water in the system, it does not conserve the amount of condensed water. In global atmospheric models, the horizontal extent of a grid column is typically tens of kilometers, large enough to host numerous clouds. GCMs keep track of the amount of water vapor Q_V , liquid water Q_L , and ice water Q_I in each grid cell, along with the cloud-fraction A indicating that only a fraction of the grid cell is cloudy while the rest remains unsaturated.

LEM's on the other hand, generally assume that the grid cells are either uniformly cloudy or unsaturated. Therefore cloud condensation only occurs if the grid cell is super-saturated by an all-or-nothing procedure. This allows the use of total specific humidity q_t , i.e the sum of condensed water and water vapor, as a prognostic variable from which the condensed water is only determined diagnostically. Virtually all atmospheric LEMs (e.g. SAM Khairoutdinov *et al.* [2005], DALES Heus *et al.* [2010], PALM [Maronga *et al.*, 2015], microHH [van Heerwaarden *et al.*, 2017], NICAM and SCALE [Tomita, 2008], and UCLALES [Stevens *et al.*, 2005]) use q_t as a prognostic variable.

In SP schemes, the q_t variable of the LEM is forced towards the total specific humidity of the global model. If q_t increases above its saturation value, clouds will form in the LEM. However, GCM grid cells containing both clouds and unsaturated air are usually unsaturated on average, and as a result the LEM will be forced towards a cloud-free state, even though the GCM column contains clouds.

It is difficult to couple the amount of cloud condensed water in the same way as the other coupled quantities in a SP setup, as it is not a prognostic variable in the LEM but

226 diagnosed from the local total specific humidity for each cell and time step. The amount
 227 of clouds in the LEM thus depends on fluctuations in state variables in the horizontal di-
 228 rection, which is a degree of freedom that so far is left uncoupled in SP schemes. In other
 229 words, the information contained in the GCM variables Q_L , Q_I and A is not transferred to
 230 the LEM in a standard SP scheme, since the LEM does not have corresponding prognostic
 231 variables to couple with these quantities.

232 Since clouds consist of local regions with higher humidity and/or lower temperature
 233 than their surroundings, we suggest that a way to control the cloudiness of the LEM is
 234 to nudge not just the horizontal average of the variables (as usually done in SP) but also
 235 the magnitude of their fluctuations from the average, in order to match the cloud-related
 236 variables of the large-scale model. This can be done in a way that leaves the fundamental
 237 relation (1) unchanged. A method to do so is described in section 3.

238 Note that even without adjusting the horizontal fluctuations, the LEM can generate
 239 clouds through convection if the conditions are favorable. The difficulties described above
 240 appear only when existing clouds in the global model should be advected into a model
 241 column with an embedded LEM, which happens to be cloud-free.

242 3 Variability coupling procedure

243 In order to couple the cloud water content of the LEM with the global model, we
 244 propose an extension to the SP coupling scheme to influence not just the horizontal av-
 245 erages but also the horizontal variability. In particular, by changing the amplitude of the
 246 fluctuations of the total specific humidity in each horizontal grid plane, the condensed wa-
 247 ter amounts there will be influenced. If the fluctuations are adjusted without altering the
 248 horizontal average, this scheme is still compatible with the superparameterization proce-
 249 dure. In other words, our proposed humidity variability coupling scheme amounts to re-
 250 distributing the total water content of each horizontal layer in the LEM, in such a way that
 251 the condensed water content matches the value from the GCM for each layer.

252 This adjustment scheme is in the spirit of the traditional SP formulation, where the
 253 two models are forced towards each other during each time step. Our scheme extends this
 254 idea to the condensed water content, which the traditional scheme doesn't couple from the
 255 GCM to the LEM. Coupling cloud condensate information in the other direction, from the
 256 LEM to the GCM, is easily handled: the forcing on the GCM can be derived from the
 257 diagnosed specific condensed water humidity q_c of the LEM.

258 3.1 Humidity variability

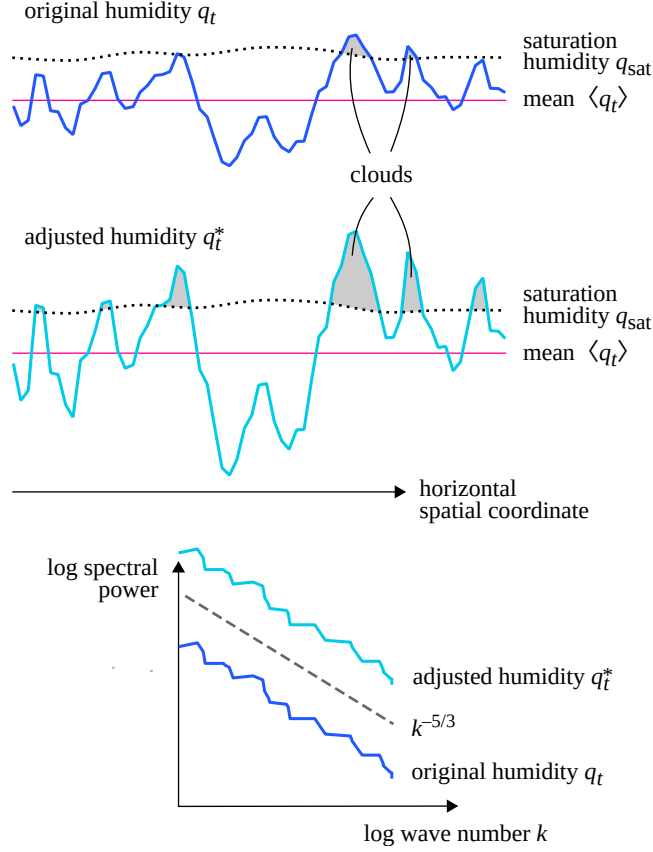
259 There are many ways to adjust the total humidity field - any perturbation which
 260 leaves the horizontal average unchanged, and does not introduce negative humidity val-
 261 ues could be considered. We choose to scale the amplitude of existing variations in each
 262 horizontal layer. In this way, we do not have to specify the length scales of the variability
 263 we add, but merely amplify the existing variability, as illustrated in figure 4. Let q_t be the
 264 total humidity, and q_{sat} the saturation humidity for each cell in the LEM. The condensed
 265 water humidity is then

$$266 q_c = \max[0, q_t - q_{\text{sat}}(p, T)]. \quad (8)$$

270 The modified q_t field can be written as

$$271 q_t^* = \beta(q_t - \langle q_t \rangle) + \langle q_t \rangle \quad (9)$$

272 where β is a scaling factor, chosen separately for each horizontal layer. If $\beta = 0$ all varia-
 273 tions of q_t around its mean are removed, if $\beta = 1$ q_t is left unchanged, and for $\beta > 1$ the
 variability is amplified. This scaling leaves the average of q_t unchanged. A consequence



259 **Figure 4.** Illustration of the variability coupling procedure. Cells where q_t is above q_{sat} are saturated, and
 260 and contribute to the condensed water content. The condensed water amount in each horizontal slab is controlled
 261 by adjusting the amplitude of the q_t fluctuations around the mean $\langle q_t \rangle$. This procedure preserves the shape
 262 (typically a $-5/3$ slope) of the humidity power spectrum.

274 of this manner of adjusting the variability is that the spatial Fourier spectrum of the q_t -
 275 field retains its shape, only the amplitude is changed. Another choice we make here is to
 276 keep the temperature T in each grid cell unchanged while adjusting q_t , which requires ad-
 277 justing the liquid water potential temperature θ_l . This choice, which is further discussed
 278 below, has an important consequence for the coupling procedure, namely that the satura-
 279 tion humidity q_{sat} in each grid cell, which depends on temperature and pressure, remains
 280 unchanged during the adjustment.

281 Next we determine β so that the average condensed water humidity q_c in the hori-
 282 zontal layer matches the condensed water humidity $Q_C = Q_L + Q_I$ of the GCM,

$$Q_C = \langle q_c(\beta) \rangle = \langle \max[0, q_t^*(\beta) - q_{\text{sat}}] \rangle. \quad (10)$$

283 Combining equations (9) and (10) gives

$$Q_C = \left\langle \max \left[0, \beta q_t + (1 - \beta) \langle q_t \rangle - q_{\text{sat}} \right] \right\rangle. \quad (11)$$

284 The max operator makes this equation difficult to handle analytically, so we solve it nu-
 285 merically for each horizontal layer.

286 3.2 Maintaining a constant temperature while coupling humidity

287 In determining the variability scaling β above, it was assumed that q_{sat} remains un-
 288 changed as β is varied. Since q_{sat} is a function of temperature and pressure, this assump-
 289 tion holds if the temperature remains constant as β is varied, as pressure is assumed to be
 290 a function only of height. In order to keep the temperature T constant while adjusting q_c ,
 291 θ_l has to be adjusted as well.

$$\Delta\theta_l = -\frac{L}{c_{pd}\Pi(p)}\Delta q_c, \quad (12)$$

292 where Δq_c is the change in cloud condensate caused by the change in q_t .

293 Also for physical reasons it is preferable to adjust the humidity while keeping the
 294 temperature constant. In cloud parameterization schemes, it is generally assumed that vari-
 295 ability in humidity is decisive for cloud formation, while variability in temperature plays
 296 a minor role [*Price and Wood, 2002*]. When adjusting the variability of the humidity, we
 297 change the condensed water content of the local model. There is no latent heat or temper-
 298 ature change associated with this re-distribution, in the same way as advection of clouds
 299 from one grid cell to another leaves the temperature unaffected.

300 3.3 Implementation details

301 While the coupling tendencies on the local models in an SP setup are generally ap-
 302 plied gradually over time, we have implemented the variability changes instantly at every
 303 time step of the large-scale model. One reason for this is that the small-scale fields move
 304 due to advection over the course of one large-scale time step, which means that the ten-
 305 dencies need to move as well in order to achieve the desired final structure. Also with an
 306 instant adjustment, it is easier to verify that the procedure actually achieves the correct
 307 cloud condensate amounts.

308 Some practical issues in the adjustment procedure need to be handled:

309 1) Equation (11) for β may give an unreasonably large β as the solution. As this
 310 can make the local model unstable, we restrict β to the range $0 \dots 5$. The permissible
 311 range of β is typically exceeded when large-scale advection would add clouds above the
 312 boundary layer, where the local model has a small variability in the horizontal direction.
 313 In this case, we add white noise to q_t , again with the amplitude selected to give the de-
 314 sired amount of cloud condensate.

315 2) q_t is not allowed to become negative in the adjustment. We have found that when
 316 limiting β as above, the procedure does not cause negative q_t values. As a precaution, one
 317 can set negative q_t values to 0, and adjust the other cells in the same horizontal layer to
 318 conserve the total mass of water.

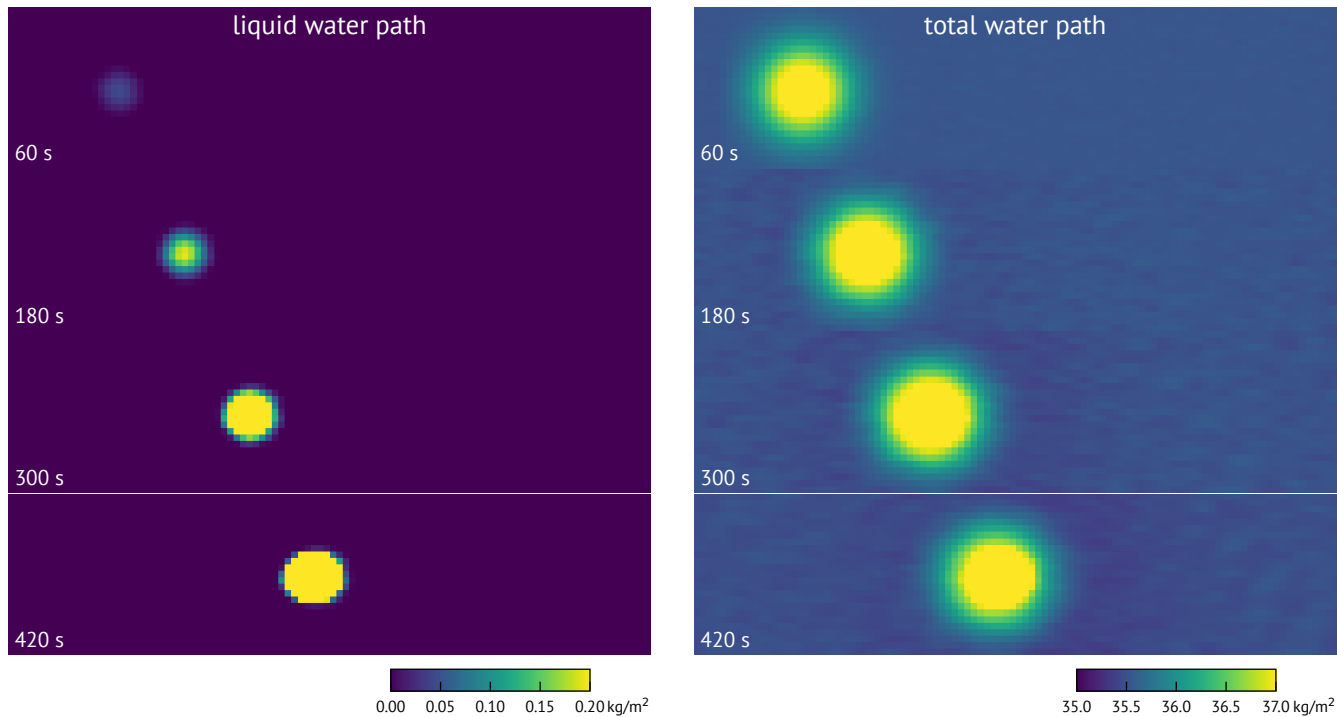
319 3) If $Q_C = 0$, β is not uniquely determined. If q_c is also 0, we set $\beta = 1$, implying
 320 no variability adjustment. If $q_c > 0$ we nudge the layer towards just below saturation i.e.
 321 $\beta < 1$ but as large as possible.

322 4) With OpenIFS as the global model, sometimes Q_C is positive but tiny, on the
 323 order of 10^{-12} kg/kg. We choose to ignore condensed water humidities $< 10^{-9}$ kg/kg,
 324 when they would result in a nudge towards more variability.

325 4 Advection and variability coupling in a simplified SP setup

326 To illustrate the problems with cloud advection in SP as well as the solutions and
 327 limitations provided by the proposed humidity variability coupling scheme, we show a
 328 simplified SP setup where the large-scale model consists of only (upwind) advection of
 329 the prognostic variables, with a fixed large-scale wind. We construct this model as a re-
 330 alization of the following thought experiment: consider an SP simulation where a single

331 LEM contains a cloud but has an average humidity below saturation, and ask if or how
 332 this cloud can be advected into an LEM at a neighboring grid point. This model provides
 333 a simple setting to illustrate the cloud advection problem in SP and to see how the vari-
 334 ability coupling approach mitigates the problem.

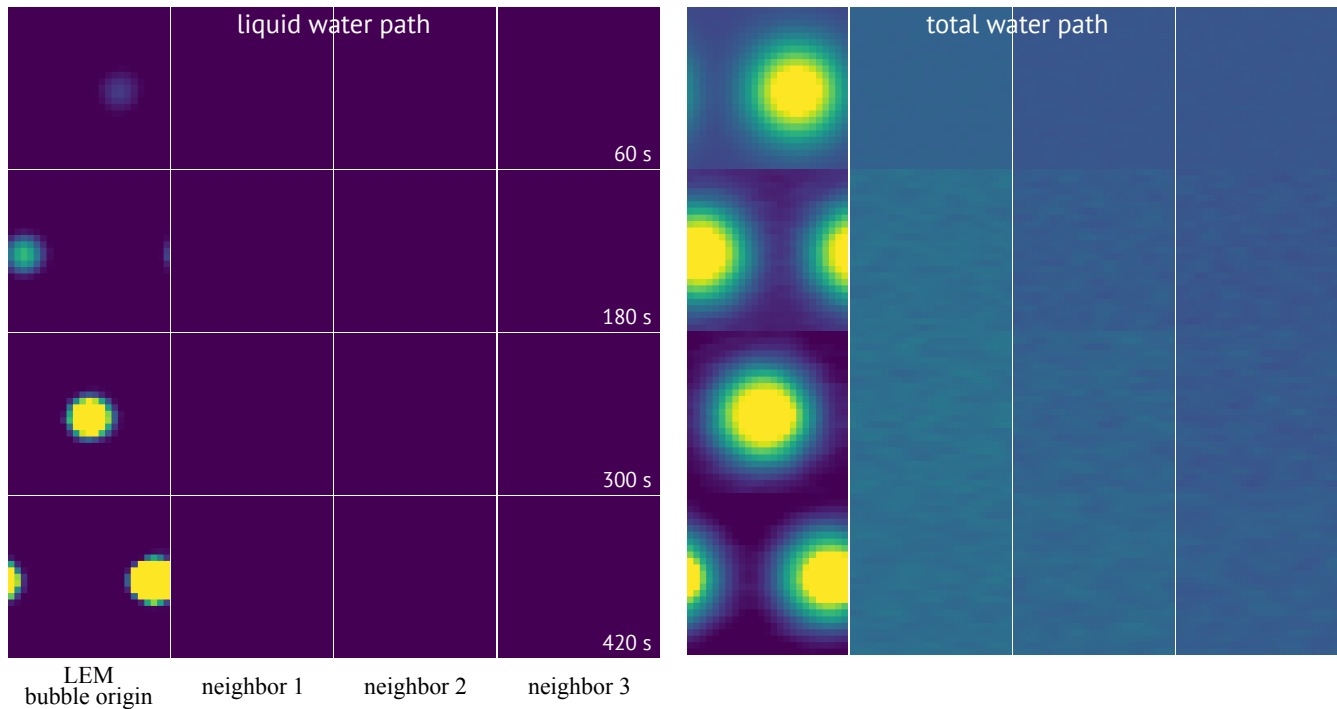


335 **Figure 5.** A moist-bubble experiment with a single large-eddy simulation domain. The plots show the
 336 liquid water path and total water path.

339 The ideal behavior in this experiment is shown in figure 5 with a single wide LEM.
 340 A superparameterized version is shown in figure 6, with four LEMs placed side by side.
 341 The LEMs are initialized with vertical profiles from the BOMEX case included with the
 342 DALES model. The left-most LEM is perturbed with a bubble of moist air, chosen to de-
 343 velop into a single cloud. There is a uniform wind to the right, advecting the cloud. The
 344 figure shows snapshots of the liquid water path and total water path in both simulations.
 345 In this experiment, the wind is 10 m/s to the east, the DALES domains are 2.5×2.5 km
 346 in the horizontal direction with a 100 m resolution, and 5 km high with a 40 m resolu-
 347 tion in the vertical. The initial bubble perturbation of q_t in the left-most LEM has a shape
 348 Gaussian with standard deviation of 500 m and a central amplitude of 1.5 g/kg, with the
 349 center at 800 m above the ground.

350 The experiment shows that with superparameterization, the cloud stays in the left-
 351 most LEM where it was created, cycling around the periodic boundary conditions of the
 352 domain. The large-scale advection of total humidity and temperature is not sufficient to
 353 transfer the cloud to the neighboring LEM. This experiment shows that even though the
 354 total humidity q_t is advected correctly according to the idea of SP, this is not sufficient for
 355 clouds (as measured with cloud cover or cloud condensed water content) to be advected.

358 Figure 7 shows the simplified SP setup with the same moist bubble perturbation as
 359 in figure 6. With the variability coupling scheme, we can see that clouds are advected be-
 360 tween the LEMs. The increased variability in the total water content from the variability
 361 coupling procedure can be seen in the total water path on the right.



337 **Figure 6.** A superparameterized moist-bubble experiment with four small-scale domains and where the
 338 large-scale model consists of advection only.

362 In the total water path plots, one can see how the variability coupling scheme causes
 363 an increase of spatial variability in the total water content. An animation of the three simulations
 364 with this simplified SP setup is available as supporting information S1.

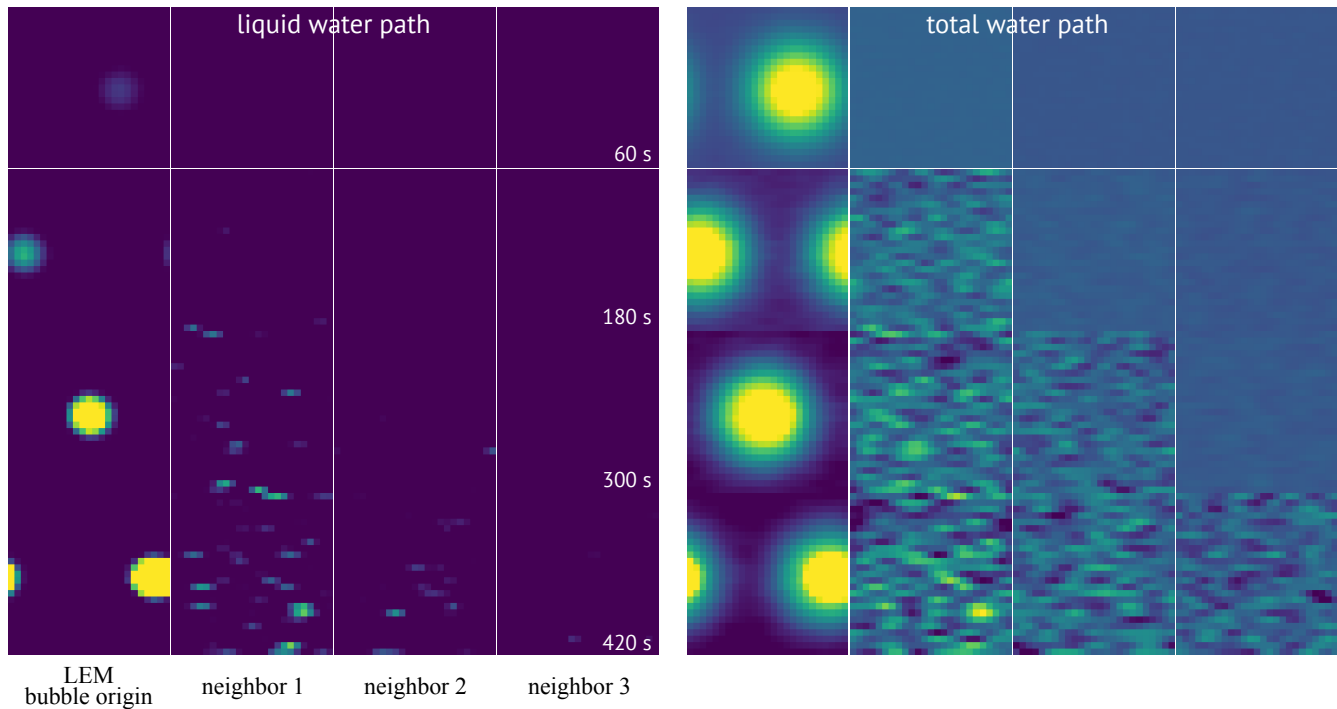
365 Even with the variability coupling, the bubble experiment is a particularly difficult
 366 case for superparameterization: the cloud in the leftmost LEM forms a single coherent
 367 structure, which is absent in the other LEMs. Figure 7 shows that the shape of the clouds
 368 is not preserved when they move between the LEMs - this would require an even more
 369 detailed coupling of the LEMs.

370 Experiments with the simplified SP model shows that the clouds added with vari-
 371 ability adjustment tend to dissipate over time — even though the adjustment initially gener-
 372 ates the desired amount of $\langle q_c \rangle$, the local models may not retain the imposed amounts
 373 of clouds when evolved in time, showing that the cloud condensate amount is a difficult
 374 property to control. This can be seen as fluctuations in the cloud condensate amount in
 375 the animation of these experiments, in supporting information S1.

376 **5 Results of superparameterized Barbados simulation with variability coupling**

377 To see the full effects of the variability coupling procedure introduced above, we
 378 repeat the Barbados simulation from section 2 with the variability coupling scheme (9)
 379 enabled.

381 Figure 8 show the Barbados simulation repeated with the variability coupling scheme.
 382 The LEMs clearly contain more clouds compared to the standard SP coupling scheme (fig-
 383 ure 1), and clouds can be advected into the SP region to a significantly higher degree than
 384 with the standard scheme. An animation comparing the three simulations shown in figures
 385 1, 3, and 8 is available as supporting information S2.



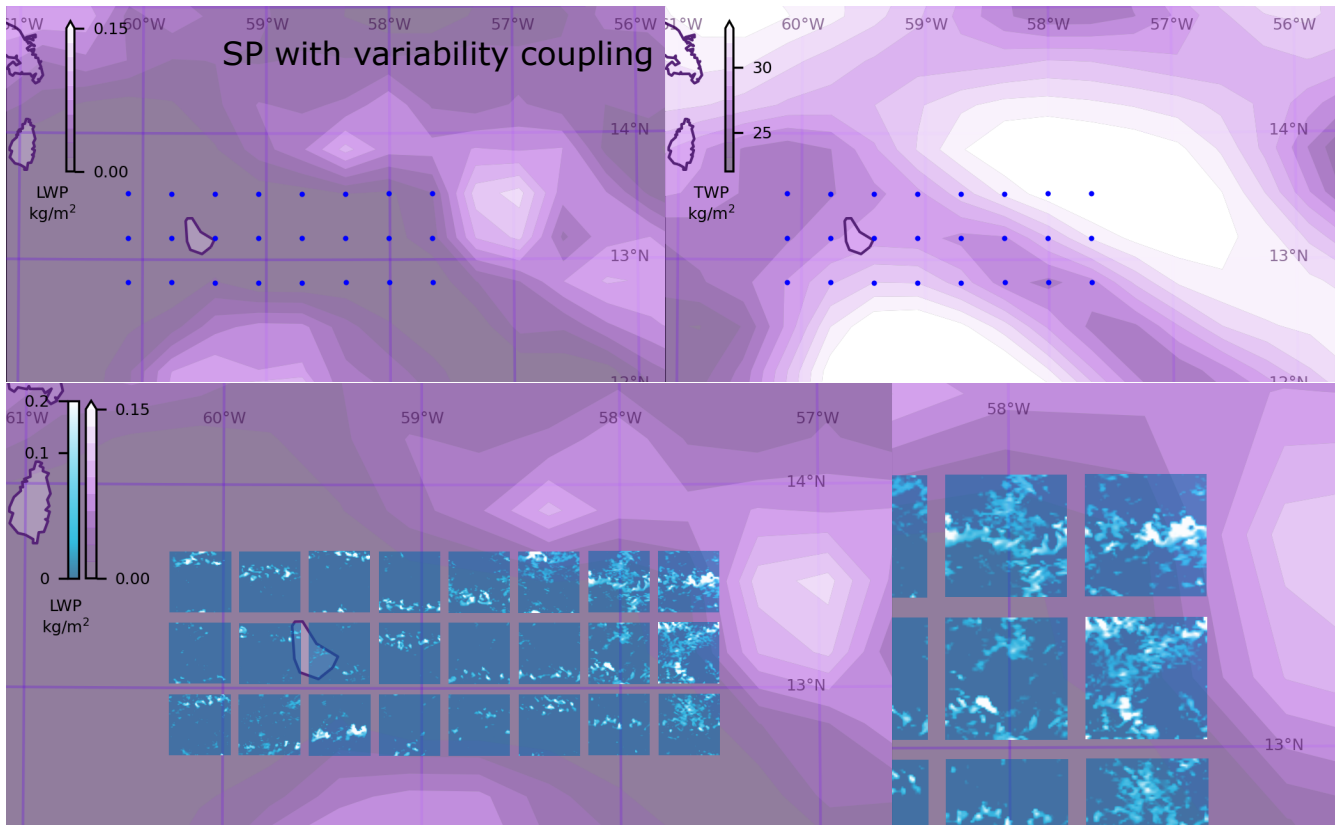
356 **Figure 7.** The moist-bubble experiment with four coupled local models shown in figure 6 repeated with
 357 variability coupling.

386 A quantitative comparison of the clouds in the three different Barbados simulations
 387 is given in figure 9, which shows east–west profiles of the liquid water path and low cloud
 388 cover. The data has been averaged over time, 04h–12h UTC, and over the north–south ex-
 389 tent of the SP domain i.e. three rows of GCM grid points. Comparing the experiments
 390 shows that SP causes a marked drop in clouds in the SP domain, both in liquid water path
 391 and in cloud cover, compared to the non-SP simulation. The variability coupling method
 392 increases the cloud content compared to standard SP, but is not sufficient to reach the lev-
 393 els of the non-SP simulation. One reason the variability coupling shows a lack of cloud
 394 condensate is that the clouds added by variability adjustment dissipate too quickly - most
 395 likely due to a lack of organization (the dissipation can be seen in the animations S1 and
 396 S2).

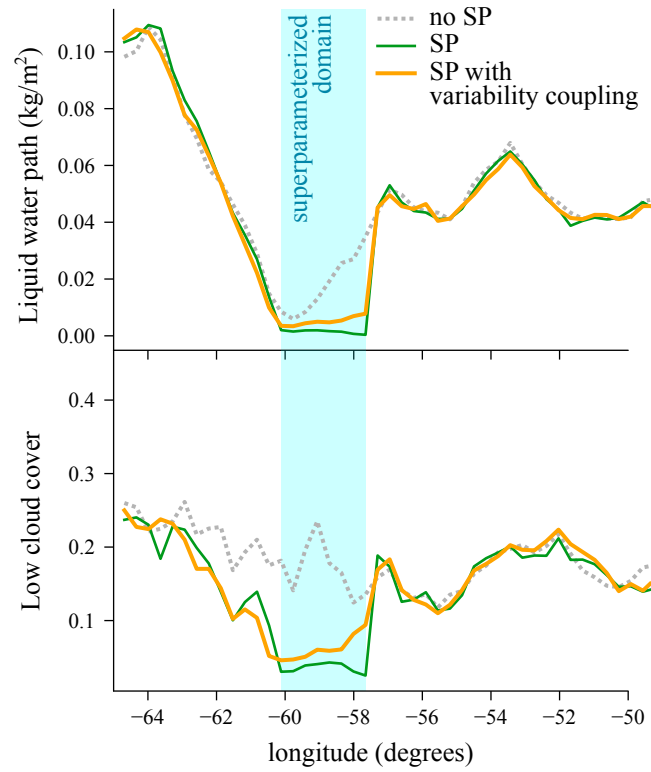
402 6 Discussion and conclusions

403 As shown in section 2.4, the difficulties of coupling cloud condensate in an SP setup
 404 are related to the global and local models being formulated using different prognostic vari-
 405 ables. The standard SP approach couples temperature, total humidity and horizontal wind
 406 velocities, which are well-defined prognostic variables in both the local and the global
 407 model. Thus one may ask if introducing prognostic cloud condensate variables in the local
 408 model would improve the situation - we argue that this is not automatically the case, and
 409 that variability related to clouds in the local model still plays a role.

410 Consider a cloud-resolving model with prognostic cloud condensate. The condensate
 411 would be advected like the other atmospheric quantities, and the model would contain ex-
 412 pressions for the conversion rates between water vapor and condensate, and between con-
 413 densate and precipitation. With such a model in an SP setup, it would be straight-forward
 414 to couple the cloud condensate between the two models in the same manner as the other



380 **Figure 8.** Superparameterization with variability coupling, in a simulation over Barbados on 2013-12-15.



397 **Figure 9.** East–west profiles of low cloud cover and liquid water path for the three Barbados simulations:
 398 no SP, SP, and SP with variability coupling. The data is averaged over 8h (04–12 UTC) and over the north–
 399 south extent of the SP domain. The SP domain is indicated with a blue background. The low cloud cover
 400 measure is from OpenIFS and is defined as the cloud cover between the surface and the height of 80% of the
 401 surface pressure (roughly 2 km). SP = superparameterization.

415 prognostic quantities. However, when a cloud is advected into a local model, the cloud
 416 condensate will be uniformly spread out in the horizontal direction. Now, if the air in this
 417 layer is not saturated, the cloud condensate will evaporate. Thus it is not only the conver-
 418 sion between different sets of prognostic variables, but the difference in representing the
 419 small-scale variations that leads to the problems in advecting clouds in an SP setup.

420 We emphasize that the issue of advecting existing clouds in an SP model is gen-
 421 eral, and not specific to our regional SP implementation. However, the regional approach
 422 clearly shows that clouds are lost when transported over the boundary between SP and
 423 non-SP regions.

424 Adjusting the small-scale variability in the local models as described in section 3
 425 improves the cloud advection in SP, but does not make the agreement in cloud condensate
 426 amounts perfect. One reason for the remaining deficiency of advected cloud condensate is
 427 that the clouds created by the variability adjustment procedure tend to shrink by evapora-
 428 tion.

429 Also regular cloud parameterizations in global models suffer from uncertainty in
 430 the small-scale structure of the clouds. With Q_V , Q_L , A known in a grid cell, the cloud
 431 processes still depend on the details of how the clouds are distributed in the grid cell on
 432 the subgrid scales. Thus, cloud advection in global models is well defined but the cloud
 433 processes are uncertain.

434 We advice caution in interpreting SP results since the advection of clouds is prob-
 435 lematic. At a minimum, SP results should be compared with the results from GLEM
 436 and other high-resolution global models that are now becoming available. [*Stevens et al.*,
 437 2019a]. Even if advection of clouds in SP is problematic, we see potential for SP as a
 438 benchmark for parameterizations, offering the possibility to compare parameterizations and
 439 cloud-resolving models under similar conditions.

440 **Acknowledgments**

441 We thank Glenn Carver at the ECMWF for help with OpenIFS and for providing us
 442 with initial states for the simulation.

443 We acknowledge the use of imagery from the NASA Worldview application
 444 (<https://worldview.earthdata.nasa.gov/>) operated by the NASA/Goddard Space Flight
 445 Center Earth Science Data and Information System (ESDIS) project.

446 This work was supported by the Netherlands eScience Center (NLeSC) under grant
 447 no. 027.015.G03. Furthermore, we acknowledge the use of ECMWF's computing and
 448 archive facilities in the research reported here. Also SURFsara provided computing re-
 449 sources.

450 **Code availability**

451 DALES, OMUSE, the SP coupler for DALES and OpenIFS, and the Simple SP ex-
 452 periment are available on GitHub under open-source licenses.

453 DALES: [*Arabas et al.*, 2021], <https://github.com/dalesteam/dales>, DOI: 10.5281/zen-
 454 odo.3759192

455 OMUSE: [*Pelupessy et al.*, 2021], <https://github.com/omuse-geoscience/omuse>, DOI:
 456 10.5281/zenodo.3755558.

457 SP coupler: [*Jansson et al.*, 2018], [https://github.com/CloudResolvingClimateModeling/sp-](https://github.com/CloudResolvingClimateModeling/sp-coupler)
 458 coupler, DOI: 10.5281/zenodo.1968304.

459 The simple SP experiment: [Jansson *et al.*, 2021], [https://github.com/CloudResolvingClimateModeling/Simple-](https://github.com/CloudResolvingClimateModeling/Simple-SP)
 460 SP DOI: 10.5281/zenodo.5511753

461 For OpenIFS, a license can be requested from ECMWF. For details of the SP setup
 462 with OpenIFS with DALES, see also Jansson *et al.* [2019]. The Python interface to DALES
 463 using OMUSE is described in van den Oord *et al.* [2020].

464 **Author contributions**

465 DC and PS conceived of the project. FJ, GvdO, DC, PS defined the SP coupling
 466 procedure. FJ, GvdO, IP, MC wrote the superparameterization coupler and Python inter-
 467 faces to OpenIFS and DALES. FJ ran the simulations. JHG and FJ developed the visual-
 468 izations. JHG drew the figures. FJ wrote the article text, with contributions and editing by
 469 all other authors.

470 **References**

- 471 Arabas, S., S. Axelsen, J. Attema, C. Beets, S. J. Boeing, M. de Bruine, J. Chylik,
 472 H. Cuijpers, J. van der Dussen, C. van Heerwaarden, T. Heus, F. Jansson, H. Jonker,
 473 A. Moene, H. Ouwersloot, G. van den Oord, S. de Roode, R. Neggers, X. Pe-
 474 druzo, P. Siebesma, M. Sikma, B. van Stratum, J. Vila, and M. van Zanten (2021),
 475 dalesteam/dales: Dales 4.3, doi:10.5281/zenodo.4604726.
- 476 Arakawa, A., J.-H. Jung, and C.-M. Wu (2011), Toward unification of the multiscale mod-
 477 eling of the atmosphere, *Atmospheric Chemistry and Physics*, 11(8), 3731–3742, doi:
 478 10.5194/acp-11-3731-2011.
- 479 Arakawa, A., J.-H. Jung, and C.-M. Wu (2016), Multiscale modeling of the moist-
 480 convective atmosphere, *Meteorological Monographs*, 56, 16.1–16.17, doi:
 481 10.1175/AMSMONOGRAPHS-D-15-0014.1.
- 482 Bony, S., B. Stevens, F. Ament, S. Bigorre, P. Chazette, S. Crewell, J. Delanoë,
 483 K. Emanuel, D. Farrell, C. Flamant, S. Gross, L. Hirsch, J. Karstensen, B. Mayer,
 484 L. Nuijens, J. H. Ruppert, I. Sandu, P. Siebesma, S. Speich, F. Szczap, J. Totems,
 485 R. Vogel, M. Wendisch, and M. Wirth (2017), EUREC4A: A field campaign to eluci-
 486 date the couplings between clouds, convection and circulation, *Surveys in Geophysics*,
 487 38(6), 1529–1568.
- 488 Grabowski, W. W. (2001), Coupling cloud processes with the large-scale dy-
 489 namics using the cloud-resolving convection parameterization (CRCP),
 490 *Journal of the Atmospheric Sciences*, 58(9), 978 – 997, doi:10.1175/1520-
 491 0469(2001)058<0978:CCPWTL>2.0.CO;2.
- 492 Grabowski, W. W. (2004), An improved framework for superparameterization,
 493 *Journal of the Atmospheric Sciences*, 61(15), 1940–1952, doi:10.1175/1520-
 494 0469(2004)061<1940:AIFFS>2.0.CO;2.
- 495 Grabowski, W. W. (2016), Towards global large eddy simulation: Super-parameterization
 496 revisited, *Journal of the Meteorological Society of Japan. Ser. II*, 94(4), 327–344, doi:
 497 10.2151/jmsj.2016-017.
- 498 Grabowski, W. W., and P. K. Smolarkiewicz (1999), CRCP: a cloud resolving convection
 499 parameterization for modeling the tropical convecting atmosphere, *Physica D: Nonlinear*
 500 *Phenomena*, 133(1), 171–178, doi:[https://doi.org/10.1016/S0167-2789\(99\)00104-9](https://doi.org/10.1016/S0167-2789(99)00104-9).
- 501 Heus, T., C. C. van Heerwaarden, H. J. J. Jonker, A. Pier Siebesma, S. Axelsen,
 502 K. van den Dries, O. Geoffroy, A. F. Moene, D. Pino, S. R. de Roode, and J. Vilà-
 503 Guerau de Arellano (2010), Formulation of the Dutch Atmospheric Large-Eddy Sim-
 504 ulation (DALES) and overview of its applications, *Geoscientific Model Development*,
 505 3(2), 415–444, doi:10.5194/gmd-3-415-2010.
- 506 Jansson, F., G. van den Oord, and I. Pelupessy (2018), Superparameterization coupler li-
 507 brary, doi:10.5281/zenodo.1968305, programming language: Python.

- 508 Jansson, F., G. van den Oord, I. Pelupessy, J. H. Grönqvist, A. P. Siebesma, and D. Crom-
 509 melin (2019), Regional superparameterization in a global circulation model using large
 510 eddy simulations, *Journal of Advances in Modeling Earth Systems*, *11*(9), 2958–2979,
 511 doi:10.1029/2018MS001600.
- 512 Jansson, F., G. van den Oord, I. Pelupessy, M. Chertova, J. H. Grönqvist, P. Siebesma,
 513 and D. Crommelin (2021), Cloudresolvingclimatemodeling/simple-sp: v1.0, doi:
 514 10.5281/zenodo.5511753.
- 515 Khairoutdinov, M., D. Randall, and C. DeMott (2005), Simulations of the atmospheric
 516 general circulation using a cloud-resolving model as a superparameterization of
 517 physical processes, *Journal of the Atmospheric Sciences*, *62*(7), 2136–2154, doi:
 518 10.1175/JAS3453.1.
- 519 Malardel, S., N. Wedi, W. Deconinck, M. Diamantakis, C. Kuehnlein, G. Mozdzyński,
 520 M. Hamrud, and P. Smolarkiewicz (2016), A new grid for the ifs, *ECMWF Newsletter*,
 521 pp. 23–28, doi:10.21957/zwdu9u5i.
- 522 Maronga, B., M. Gryschka, R. Heinze, F. Hoffmann, F. Kanani-Sühring, M. Keck, K. Ke-
 523 telsen, M. O. Letzel, M. Sühring, and S. Raasch (2015), The parallelized large-eddy
 524 simulation model (PALM) version 4.0 for atmospheric and oceanic flows: model formu-
 525 lation, recent developments, and future perspectives, *Geoscientific Model Development*,
 526 *8*(8), 2515–2551, doi:10.5194/gmd-8-2515-2015.
- 527 Parishani, H., M. S. Pritchard, C. S. Bretherton, M. C. Wyant, and M. Khairoutdinov
 528 (2017), Toward low-cloud-permitting cloud superparameterization with explicit bound-
 529 ary layer turbulence, *Journal of Advances in Modeling Earth Systems*, *9*(3), 1542–1571,
 530 doi:https://doi.org/10.1002/2017MS000968.
- 531 Pelupessy, I., G. van den Oord, F. Jansson, M. Verstraaten, B. van Werkhoven,
 532 S. Baars, M. Chertova, and A. Candy (2021), omuse-geoscience/omuse:, doi:
 533 10.5281/zenodo.5006102.
- 534 Price, J. D., and R. Wood (2002), Comparison of probability density functions for to-
 535 tal specific humidity and saturation deficit humidity, and consequences for cloud
 536 parametrization, *Quarterly Journal of the Royal Meteorological Society*, *128*(584), 2059–
 537 2072, doi:10.1256/003590002320603539.
- 538 Satoh, M., B. Stevens, F. Judt, M. Khairoutdinov, S.-J. Lin, W. M. Putman, and P. Düben
 539 (2019), Global cloud-resolving models, *Current Climate Change Reports*, *5*(3), 172–184,
 540 doi:10.1007/s40641-019-00131-0.
- 541 Stevens, B., C.-H. Moeng, A. S. Ackerman, C. S. Bretherton, A. Chlond, S. de Roode,
 542 J. Edwards, J.-C. Golaz, H. Jiang, M. Khairoutdinov, M. P. Kirkpatrick, D. C. Lewellen,
 543 A. Lock, F. Müller, D. E. Stevens, E. Whelan, and P. Zhu (2005), Evaluation of large-
 544 eddy simulations via observations of nocturnal marine stratocumulus, *Mon. Weather*
 545 *Rev.*, *133*, 1443–1462, doi:10.1175/MWR2930.1.
- 546 Stevens, B., M. Satoh, L. Auger, J. Biercamp, C. S. Bretherton, X. Chen, P. Düben,
 547 F. Judt, M. Khairoutdinov, D. Klocke, C. Kodama, L. Kornblueh, S.-J. Lin, P. Neu-
 548 mann, W. M. Putman, N. Röber, R. Shibuya, B. Vanniere, P. L. Vidale, N. Wedi, and
 549 L. Zhou (2019a), Dyamond: the dynamics of the atmospheric general circulation mode-
 550 led on non-hydrostatic domains, *Progress in Earth and Planetary Science*, *6*(1), 61, doi:
 551 10.1186/s40645-019-0304-z.
- 552 Stevens, B., F. Ament, S. Bony, S. Crewell, F. Ewald, S. Gross, A. Hansen, L. Hirsch,
 553 M. Jacob, T. Kölling, H. Konow, B. Mayer, M. Wendisch, M. Wirth, K. Wolf, S. Bakan,
 554 M. Bauer-Pfundstein, M. Brueck, J. Delanoë, A. Ehrlich, D. Farrell, M. Forde,
 555 F. Gödde, H. Grob, M. Hagen, E. Jäkel, F. Jansen, C. Klepp, M. Klingebiel, M. Mech,
 556 G. Peters, M. Rapp, A. A. Wing, and T. Zinner (2019b), A high-altitude long-range
 557 aircraft configured as a cloud observatory: The NARVAL expeditions, *Bulletin of the*
 558 *American Meteorological Society*, *100*(6), 1061 – 1077, doi:10.1175/BAMS-D-18-
 559 0198.1.
- 560 Stevens, B., S. Bony, D. Farrell, F. Ament, A. Blyth, C. Fairall, J. Karstensen, P. K.
 561 Quinn, S. Speich, Acquistapace, et al. (2021), EUREC⁴A, *Earth System Science Data*,

- 562 *13*(8), 4067–4119, doi:10.5194/essd-13-4067-2021.
- 563 Tomita, H. (2008), New microphysical schemes with five and six categories by diagnos-
564 tic generation of cloud ice, *Journal of the Meteorological Society of Japan. Ser. II*, *86A*,
565 121–142, doi:10.2151/jmsj.86A.121.
- 566 van den Oord, G., F. Jansson, I. Pelulessy, M. Chertova, J. H. Grönqvist, P. Siebesma, and
567 D. Crommelin (2020), A Python interface to the Dutch atmospheric large-eddy simula-
568 tion, *SoftwareX*, *12*, 100,608, doi:10.1016/j.softx.2020.100608.
- 569 van Heerwaarden, C. C., B. J. H. van Stratum, T. Heus, J. A. Gibbs, E. Fedorovich, and
570 J. P. Mellado (2017), MicroHH 1.0: a computational fluid dynamics code for direct
571 numerical simulation and large-eddy simulation of atmospheric boundary layer flows,
572 *Geoscientific Model Development*, *10*(8), 3145–3165, doi:10.5194/gmd-10-3145-2017.